Anomalous low-temperature physical properties of the ytterbium-based Kondo-lattice compounds Yb_4TGe_8 (T = Cr, Mn, Fe, Co, and Ni)

Shunsuke Yamanaka,[1] Masahito Hikiji,[1] Chishiro Michioka,[1,*] Hiroaki Ueda,[1] Akira Matsuo,[2] Koichi Kindo,[2] Hitoshi Yamaoka,[3] Naohito Tsujii,[4] and Kazuyoshi Yoshimura[1]

[1]*Department of Chemistry, Graduate School of Science, Kyoto University, Kyoto 606-8502, Japan*
[2]*Institute for Solid State Physics, The University of Tokyo, Kashiwanoha, Kashiwa, Chiba 277-8581, Japan*
[3]*RIKEN SPring-8 Center, Sayo, Hyogo 679-5148, Japan*
[4]*International Center for Materials Nanoarchitectonics (MANA), National Institute for Materials Science, Tsukuba, Ibaraki 305-0047, Japan*

(Received 23 April 2021; revised 14 June 2022; accepted 14 June 2022; published 1 July 2022)

In this study, we have prepared single crystals of ytterbium-based layered compounds Yb_4TGe_8 (T = Cr, Mn, Fe, Co, and Ni) and investigated their magnetic, thermal, and transport properties systematically. The magnetic properties for all the five compounds show a typical behavior for the Kondo-lattice system at high temperatures and are highly anisotropic due to orbital moments in the degenerate ground state. At low temperatures, an additional magnetic correlation enhances the magnetic susceptibility, and both the heat capacity and the electrical resistivity deviate from the Fermi-liquid-like behavior. Such unconventional behaviors at low temperatures are discussed considering a contribution of strongly correlated characters in T atoms to the conduction band.

DOI: 10.1103/PhysRevB.106.024402

I. INTRODUCTION

Ytterbium- and cerium-based metallic compounds often have strong electron correlations, and they have been subjected to extensive researches and developments over the past few decades. The hybridization between conduction bands and $4f$ orbitals leads both to the Ruderman-Kittel-Kasuya-Yosida (RKKY) interaction [1–3] and the Kondo effect [4–7], and the ground state is determined by the balance of these two interactions. Doniach proposed a universal phase diagram by studying this balance [8]. Based on the phase diagram, many compounds are classified into two groups by the ground state, i.e., a magnetically ordered phase [9–16] and a nonmagnetic heavy-fermion state [17–26]. Further investigation revealed that anomalous electronic state called non-Fermi liquid [27–32] is realized in the nonmagnetic state near the magnetic quantum critical point (QCP). In non-Fermi liquid, the low-temperature behaviors of physical quantities such as magnetic susceptibility, electrical resistivity, and heat capacity deviate from the Fermi-liquid (FL) behavior, and unconventional superconductivity could be occasionally observed [33–37].

The valence state is also one of the important subjects for ytterbium- and cerium-based compounds. For cerium-based compounds, a valence fluctuation between Ce^{3+} and Ce^{4+} ions is scarcely observed near the magnetic QCP, and the magnetic properties originate in the robust Ce^{3+} ions. On the other hand, the effect of the valence fluctuation between Yb^{2+} and Yb^{3+} ions is significant even near the magnetic QCP and often remains even in the magnetically ordered state [38–45]. Therefore, detailed investigations on the valence state are required to clarify the properties near the magnetic QCP on the ytterbium-based compounds. It is revealed that the valence of ytterbium in Yb_4CrGe_8 and Yb_4MnGe_8 is approximately 2.84 at room temperature and decreases on the order of 0.08 and 0.1 toward 12 K, respectively [46].

The crystal and electric structure of Yb_4TGe_8 is reported by Peter *et al*. [47]. The crystal structure of Yb_4TGe_8 is identified based on the $CeNiSi_2$ structure type, where the Ni site is occupied by T atoms with the site occupancy of $\frac{1}{4}$. In addition, the temperature dependence of the lattice constant suggests zero thermal expansion (ZTE), where the volume is temperature independent at low temperatures. The origin of ZTE is claimed to be attributed to the unusual atomic arrangement in Yb_4TGe_8. We also studied the temperature and pressure dependencies of the electronic and crystal structures using high-resolution x-ray absorption spectroscopy, x-ray diffraction, and photoelectron spectroscopy in order to clarify the details of ZTE [46].

This paper reports the magnetic, thermal, and transport properties of ytterbium-based layered compounds Yb_4TGe_8 (T = Cr, Mn, Fe, Co, and Ni) investigated using single crystals. The five compounds exhibit typical physical properties for the Kondo-lattice system above 10 K, while an additional magnetic correlation develops at low temperatures, resulting in different low-temperature physical properties for each compound. The most striking feature of Yb_4TGe_8 is the presence of T atoms with $3d$ electrons in addition to Yb atoms exhibiting localized magnetism. The carrier density changes depending on the T atoms and varies the low-temperature physical properties of Yb_4TGe_8 (T = Cr, Mn, Fe, Co, and Ni).

*michioka@kuchem.kyoto-u.ac.jp

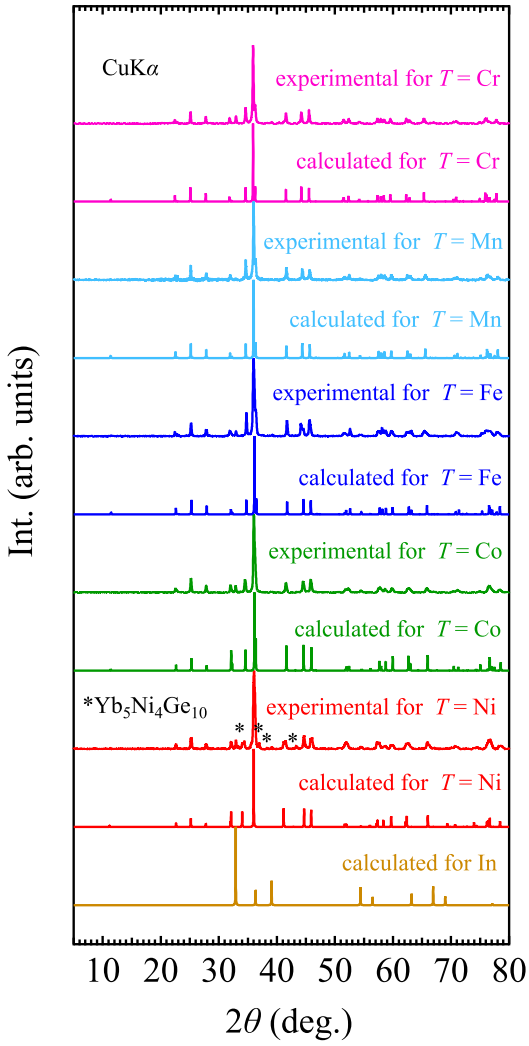

FIG. 1. Powder x-ray diffraction patterns for Yb_4TGe_8 (T = Cr, Mn, Fe, Co, and Ni) at room temperature and the calculated patterns for Yb_4TGe_8 (T = Cr, Mn, Fe, Co, and Ni) and indium.

II. EXPERIMENT

Single crystals of Yb_4TGe_8 (T = Cr, Mn, Fe, Co, and Ni) were grown using an indium flux method [47]. The starting materials were Yb ingot (Rare Metallic, 99.9%), Cr powder (Rare Metallic, 99.9%), Mn flake (Rare Metallic, 99.99%), Fe granular (Aldrich, 99.995%), Co shot (Rare Metallic, 99.9%), Ni granular (Rare Metallic, 99.993%), Ge ingot (Rare Metallic, 99.999%), and In ingot (Rare Metallic, 99.99%). The materials were enclosed in a Tammann tube (alumina purity: 99.7%) and placed in a sealed quartz tube under an argon pressure of 0.3 atm. The quartz tube was heated up to 1100 °C for Yb_4MnGe_8 and up to 1000 °C for the other compounds and then slowly cooled. The indium flux surrounding the grown crystals was removed by centrifugation and hydrochloric acid etching. Flat platelike single crystals were obtained with typical sizes of $3.0 \times 0.5 \times 0.5$, $3.0 \times 1.5 \times 1.0$, $0.7 \times 0.2 \times 0.1$, $1.7 \times 0.3 \times 0.2$, and $1 \times 0.5 \times 0.5$ mm^3 for Yb_4TGe_8 (T = Cr, Mn, Fe, Co, and Ni), respectively.

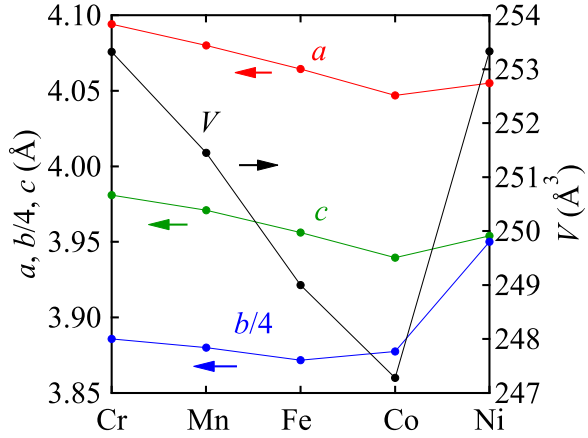

FIG. 2. Lattice constants a, b, and c and the unit-cell volume V for Yb_4TGe_8 (T = Cr, Mn, Fe, Co, and Ni).

The crushed and powdered samples were characterized using powder x-ray diffraction (XRD) with Cu $K\alpha$ radiation at room temperature using Rigaku MiniFlex 600. POWDER CELL analysis [48] was performed to estimate the crystallographic parameters. The chemical composition was estimated using energy-dispersive x-ray spectroscopy (EDX) in conjunction with scanning electron microscopy (SEM) with averaging data of several spots in a crystal.

The temperature dependence of the magnetic susceptibility was measured under the magnetic field of 1 T between 2 and 300 K using a quantum design magnetic property measurement system (MPMS) at the Research Center for Low Temperature and Materials Sciences, Kyoto University. Magnetization curves at 4.2 K up to 60 T were measured using a multilayer pulsed magnet at the International MegaGauss Science Laboratory of the Institute for Solid State Physics at University of Tokyo. The heat-capacity measurements were performed with a relaxation method under the magnetic field of 0 to 14 T between 2 and 200 K by using a quantum design physical property measurement system (PPMS). Electrical resistivity measurements were performed with a standard four-probe method under the magnetic field of 0 to 14 T between 2 and 300 K using a quantum design PPMS.

III. RESULTS

A. Structural properties

Figure 1 shows powder XRD patterns for Yb_4TGe_8 (T = Cr, Mn, Fe, Co, and Ni) at room temperature and the calculated patterns for these compounds and indium [49]. The calculated patterns for Yb_4TGe_8 are obtained by refining powder XRD patterns for Yb_4TGe_8 based on the data calculated for $DyCr_{0.25}Ge_2$ [50]. The asterisks in Fig. 1 show an impurity peak of $Yb_5Ni_4Ge_{10}$ [51]. Powder XRD patterns for Yb_4TGe_8 are in good agreement with the calculated patterns for Yb_4TGe_8 except for small impurity phases of indium used as a flux and $Yb_5Ni_4Ge_{10}$ in Yb_4NiGe_8. Since the amount of indium estimated from powder XRD patterns for Yb_4TGe_8 is small and indium is nonmagnetic, it would not significantly affect the other measurements. For Yb_4NiGe_8, a sufficient amount of single crystals could not be obtained for powder

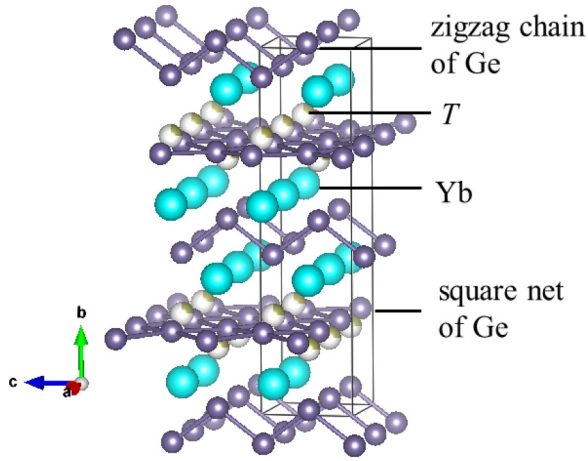

FIG. 3. Crystal structure of Yb_4TGe_8 (T = Cr, Mn, Fe, Co, and Ni).

XRD measurement. Therefore, the polycrystals that were synthesized with the single crystals were also crushed together with single crystals and used for powder XRD measurement. The impurity phase was contained in these polycrystals. The absence of the impurity phase in each single crystal was confirmed by EDX analysis as shown later. The lattice constants a, b, and c and the unit-cell volume V for Yb_4TGe_8 (T = Cr, Mn, Fe, Co, and Ni) are shown in Fig. 2. They tend to decrease with decreasing the ionic radius of the T atom except for Yb_4NiGe_8. This is consistent with the report by Peter *et al.* [47], in which this anomalous elongation of the b axis in Yb_4NiGe_8 is attributed to the different degree of distortions in the zigzag chain and the square net of Ge atoms in Yb_4NiGe_8 compared with those of the other compounds.

The crystal structure of Yb_4TGe_8 (T = Cr, Mn, Fe, Co, and Ni) is shown in Fig. 3, where Yb atoms are sandwiched between zigzag chains and a square net of Ge atoms to form a layered structure, and T atoms are alternately stacked on the top and bottom of the square net with a site occupancy of $\frac{1}{4}$. Since Yb atoms in Yb_4TGe_8 occupy a single crystallographic site, the anomalous physical properties at low temperatures, which will be discussed later, do not result from multiple Yb sites.

The chemical compositions of single crystals of Yb_4TGe_8 (T = Cr, Mn, Fe, Co, and Ni) estimated from EDX are listed in Table I. The EDX analysis is sensitive to surface condition of measured samples and have a measurement error from 10% to 20%. Within the measuring error, the composition of the five compounds would be close to the ideal composition Yb : T : Ge = 4 : 1 : 8.

TABLE I. Chemical compositions of Yb_4TGe_8 (T = Cr, Mn, Fe, Co, and Ni) estimated from EDX.

	Cr	Mn	Fe	Co	Ni
Yb	4.28	3.97	3.76	3.80	3.21
T	1.03	0.96	0.91	1.15	0.94
Ge	7.72	8.03	8.24	8.20	8.79

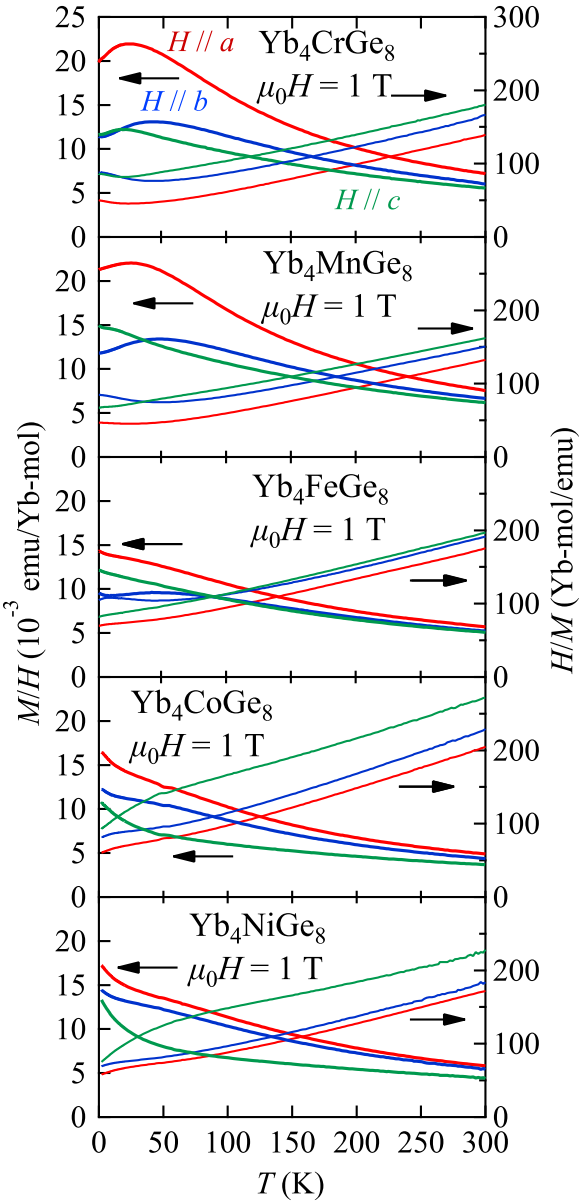

FIG. 4. Temperature dependence of the magnetic susceptibility M/H and its inverse H/M in Yb_4TGe_8 (T = Cr, Mn, Fe, Co, and Ni) under $\mu_0 H = 1$ T for $H \parallel a$, b, and c.

B. Magnetic properties

Figure 4 shows the temperature T dependence of magnetic susceptibility $M/H = \chi$ and its inverse $H/M = \chi^{-1}$ in Yb_4TGe_8 (T = Cr, Mn, Fe, Co, and Ni) under $\mu_0 H = 1$ T for $H \parallel a$, b, and c directions, where M is the magnetization, H is the magnetic field, and μ_0 is the magnetic permeability of vacuum. For all the five compounds, M/H shows a characteristic anisotropic behavior, which is attributed to the anisotropic orbital momentum in the degenerated ground state. The temperature dependence of M/H obeys the Curie-Weiss law above 150 K. The effective magnetic moment $\mu_{\rm eff}$ and the Weiss temperature $\theta_{\rm W}$ estimated from the Curie-Weiss fit between 150 and 300 K are listed in Table II. All $\mu_{\rm eff}$ roughly agree with the theoretical value for the free Yb^{3+} ion of 4.54 $\mu_{\rm B}$, suggesting the localized

TABLE II. Values of the effective magnetic moment $\mu_{\rm eff}$ and the Weiss temperature $\theta_{\rm W}$ estimated from the Curie-Weiss fit. The numbers in parentheses are the standard deviations in the last significant figures.

T	Direction	$\mu_{\rm eff}$ ($\mu_{\rm B}$/Yb)	$\theta_{\rm W}$ (K)
	$H\|\|a$	4.477(3)	−47.8(3)
Cr	$H\|\|b$	4.426(10)	−101.0(15)
	$H\|\|c$	4.487(6)	−151.5(10)
	$H\|\|a$	4.621(2)	−52.4(3)
Mn	$H\|\|b$	4.753(2)	−124.5(4)
	$H\|\|c$	4.777(3)	−161.4(6)
	$H\|\|a$	4.423(3)	−127.2(5)
Fe	$H\|\|b$	4.333(7)	−147.9(12)
	$H\|\|c$	4.320(2)	−158.6(4)
	$H\|\|a$	3.806(4)	−69.4(6)
Co	$H\|\|b$	3.684(4)	−85.9(7)
	$H\|\|c$	3.832(5)	−198.0(12)
	$H\|\|a$	4.264(4)	−90.4(5)
Ni	$H\|\|b$	4.219(8)	−105.9(13)
	$H\|\|c$	4.489(15)	−265(3)

character of $4f$ electrons. The Yb valence and χT in Yb_4CrGe_8 and Yb_4MnGe_8 are compared as function of temperature between 12 and 300 K, and nice agreement is observed [46]. This suggests that the static magnetization is dominated not by the $3d$ electrons from T atoms but by $4f$ electrons in Yb atoms. Although the effect of the crystalline electric field (CEF) prevents us from estimating the strength of the magnetic interaction from $\theta_{\rm W}$, the fact that each $\theta_{\rm W}$ is negative in all directions of the applied magnetic fields suggests that the dominant magnetic interaction is antiferromagnetic.

In Yb_4CrGe_8, a broad maximum is observed for $H \parallel a$, b, and c, while no magnetic ordering is observed in the heat-capacity measurements as shown later. Therefore, the broad maximum would result from screening accompanied by the Kondo singlet formation. In addition, an additional magnetic correlation develops at low temperatures and makes the behavior of M/H for the five compounds different. In the M/H-T curves of Yb_4MnGe_8 for $H \parallel c$ and of Yb_4FeGe_8 for $H \parallel a$ and c, the broad maximum is masked by the enhancement of M/H caused by the additional magnetic correlation. In Yb_4CoGe_8 and Yb_4NiGe_8, the large contribution of the additional magnetic correlation to M/H also masks a broad maximum behavior of M/H for all the applied magnetic field directions.

The temperature at which M/H achieves the maximum $T_\chi^{\rm max}$ is a guide for $T_{\rm K}$, and it indicates the distance from the magnetic QCP. To clarify the value of $T_\chi^{\rm max}$ and the behavior of M/H at low temperatures, we replot the temperature dependence of M/H on a semilogarithmic scale, as shown in Fig. 5. The value of $T_\chi^{\rm max}$ slightly depends on the direction of the applied magnetic field. Here, we employ the data for $H \parallel b$, in which $T_\chi^{\rm max}$ for Yb_4CrGe_8, Yb_4MnGe_8, and Yb_4FeGe_8 can be determined separately from the enhancement of M/H at low temperatures. The values of $T_\chi^{\rm max}$ for Yb_4CrGe_8, Yb_4MnGe_8, and Yb_4FeGe_8 are 45, 49, and 46 K, respectively. In Yb_4CoGe_8 and Yb_4NiGe_8, the value of $T_\chi^{\rm max}$ cannot be precisely defined due to a drastic enhancement of

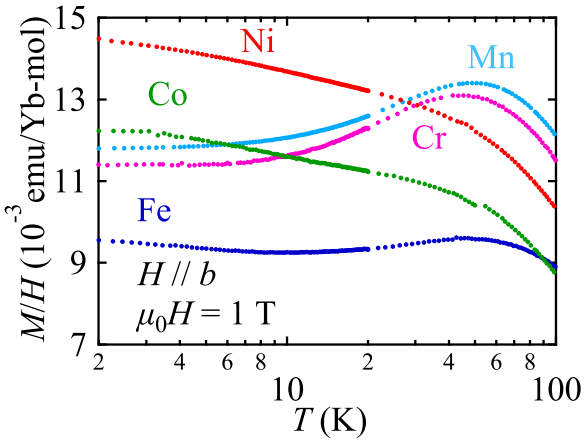

FIG. 5. M/H plotted against temperature on a semilogarithmic scale in Yb_4TGe_8 (T = Cr, Mn, Fe, Co, and Ni) under $\mu_0 H = 1$ T for $H \parallel b$ below 100 K.

M/H at low temperatures. However, the slope of the curve varies gradually between 40 and 55 K, suggesting that $T_\chi^{\rm max}$ for Yb_4CoGe_8, Yb_4NiGe_8 is comparable with Yb_4CrGe_8, Yb_4MnGe_8, and Yb_4FeGe_8. In Yb_4CrGe_8, Yb_4MnGe_8, and Yb_4FeGe_8, M/H approaches temperature-independent behavior below $T_\chi^{\rm max}$. On the other hand, M/H in Yb_4CoGe_8 and Yb_4NiGe_8 is enhanced at low temperatures.

The magnetization curves for $H \parallel a$, b, and c measured at 4.2 K are shown in the Supplemental Material [52]. The value of M does not reach the theoretical value for the free Yb^{3+} ion of 4 $\mu_{\rm B}$ even under $\mu_0 H = 60$ T.

C. Heat capacity

The insets in Fig. 6 show the temperature dependence of C_p/T in Yb_4TGe_8 (T = Cr, Mn, Fe, Co, and Ni) between 2 and 200 K. All the five compounds show a similar behavior except for that of low temperatures, and no anomaly indicating magnetic ordering is observed. This is consistent with the temperature dependence of M/H.

Figure 6 shows the T^2 dependence of the heat capacity divided by temperature C_p/T in Yb_4TGe_8 (T = Cr, Mn Fe, Co, and Ni). The solid lines show data fit with the function $C_p/T = \gamma + \beta T^2$ between 9 and 15 K, where γ is the Sommerfeld constant and β is a parameter related to the phonon contribution to the heat capacity. The Debye temperature $\theta_{\rm D}$ is associated with β as $\theta_{\rm D} = (\frac{12\pi^4 nR}{5\beta})^{1/3}$, where R is the gas constant and n is the number of atoms per formula unit which is $\frac{13}{4}$ for the present compounds. The values of β, $\theta_{\rm D}$, and γ are listed in Table III. Although this fit function is useful for low temperatures, where the phonon contribution to the heat capacity should be $\sim T^3$ in the Debye model, the data in all the five compounds deviates from this function at low temperatures. This is possibly due to the additional magnetic correlation, which is also observed in the $M/H - T$ curves. The values of β estimated between 9 and 15 K are similar in all the five compounds, and the FL model with Debye phonons is adequate in this temperature range. The value of γ tends to decrease as the number of electrons in the T atom increases, suggesting a decrease in the number of conduction

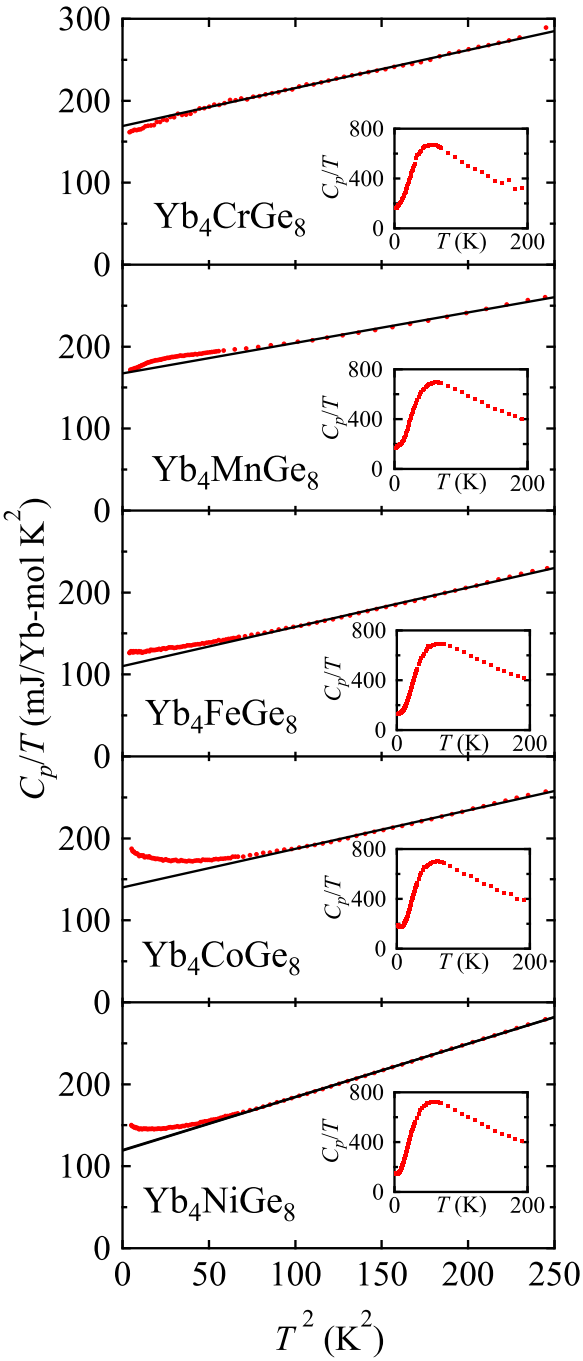

FIG. 6. T^2 dependence of the heat capacity divided by temperature C_p/T in Yb$_4T$Ge$_8$ (T = Cr, Mn Fe, Co, and Ni). The solid lines show data fit with the function $C_p/T = \gamma + \beta T^2$ between 9 and 15 K. The insets show the temperature dependence of C_p/T between 2 and 200 K.

electrons. In addition, the large $\gamma \sim 140$ mJ/mol K^2 indicates a strong electronic correlation through coupling between conduction electrons and f electrons, so-called c-f coupling. If we consider these electron correlations using the effective mass model of electrons, the effective mass decreases in Yb$_4$CrGe$_8$ and Yb$_4$MnGe$_8$ and increases in Yb$_4$FeGe$_8$, Yb$_4$CoGe$_8$, and Yb$_4$NiGe$_8$ below 9 K. The low-temperature upturn in the $C_p/T - T$ of Yb$_4$CoGe$_8$ and Yb$_4$NiGe$_8$ might

TABLE III. Values of γ, β, and the Debye temperature θ_D estimated from data fit using the function $C_p/T = \gamma + \beta T^2$, where $\theta_D = (\frac{12\pi^4 nR}{5\beta})^{1/3}$. The numbers in parentheses are the standard deviations in the last significant figures.

T	γ (mJ/mol K^2)	β (mJ/mol K^4)	θ_D (K)
Cr	169(1)	0.464(3)	239(2)
Mn	169(3)	0.366(17)	259(4)
Fe	110(2)	0.486(9)	236(2)
Co	141(2)	0.466(13)	239(3)
Ni	120(1)	0.653(3)	213(0)

be reminiscent of the tail of the Schottky anomaly. However, this upturn is suppressed with applied magnetic field as shown later, and the possibility of the Schottky anomaly originating in both the the CEF effect and the nuclear magnetic moment would be ruled out. In addition, the low-temperature state of C_p/T is dominated by the many-body effect between Yb^{3+} ions and cannot be described by the single-ion model. Therefore, the Schottky anomaly due to the CEF effect would not appear so clearly.

The Pauli paramagnetic susceptibility $\chi(0)$ is related to γ through the Wilson ratio $R_W = \frac{\chi(0)}{\gamma}\frac{4\pi^2 k_B^2}{3(g_J\mu_B)^2}$, where k_B is the Boltzmann constant, g_J is the Lande's g factor, and μ_B is the Bohr magneton. In this system, the additional magnetic correlation at low temperatures makes accurate estimation of γ and $\chi(0)$ difficult. Here, the values of C_p/T at 2 K and the average value of M/H for $H \parallel a$, b, and c at 2 K are adopted as γ and $\chi(0)$, respectively, and R_W can be roughly estimated. The estimated values of R_W for Yb$_4T$Ge$_8$ (T = Cr, Mn, Fe, Co, and Ni) are 2.0(6), 2.1(5), 2.1(4), 1.6(3), and 2.2(3), respectively. In Yb$_4$CrGe$_8$, Yb$_4$MnGe$_8$, and Yb$_4$FeGe$_8$, R_W is close to 2 which is generally observed in FL state of f-electron compounds. On the other hand, R_W for Yb$_4$CoGe$_8$ and Yb$_4$NiGe$_8$ is slightly deviated from $R_W = 2$, and the ground state would not be of a simple FL.

Figure 7 shows the temperature dependence of the electronic heat capacity divided by temperature C_e/T below 30 K, where C_e is obtained by subtracting the phonon contribution C_{ph} from C_p. To estimate C_{ph}, the heat capacity of the isostructural reference compound is corrected for molecular weight and the electronic heat capacity is subtracted from it, where Y$_4$CrGe$_8$ for Yb$_4$CrGe$_8$ and Y$_4$MnGe$_8$ for Yb$_4$MnGe$_8$, Yb$_4$FeGe$_8$, Yb$_4$CoGe$_8$, and Yb$_4$NiGe$_8$ are used as the reference. In Yb$_4$CrGe$_8$ and Yb$_4$MnGe$_8$, C_e/T slightly increases with decreasing temperature and changes to temperature-independent behavior below approximately 9 and 4 K, respectively. In Yb$_4$FeGe$_8$ and Yb$_4$CoGe$_8$, C_e/T is enhanced below 11 K after temperature-independent behavior above 11 K. In Yb$_4$NiGe$_8$, C_e/T has a broad peak around 23 K, subsequently changes to temperature-independent behavior below 9 K, and is enhanced with further decreasing temperature below 6 K. These results suggest that the development of the additional magnetic correlation in Yb$_4$CrGe$_8$ and Yb$_4$MnGe$_8$ occurs at temperatures higher than those in Yb$_4$FeGe$_8$, Yb$_4$CoGe$_8$, and Yb$_4$NiGe$_8$. In addition, the additional magnetic correlation in Yb$_4$CrGe$_8$ and Yb$_4$MnGe$_8$ is suppressed at low temperatures, while such a correlation

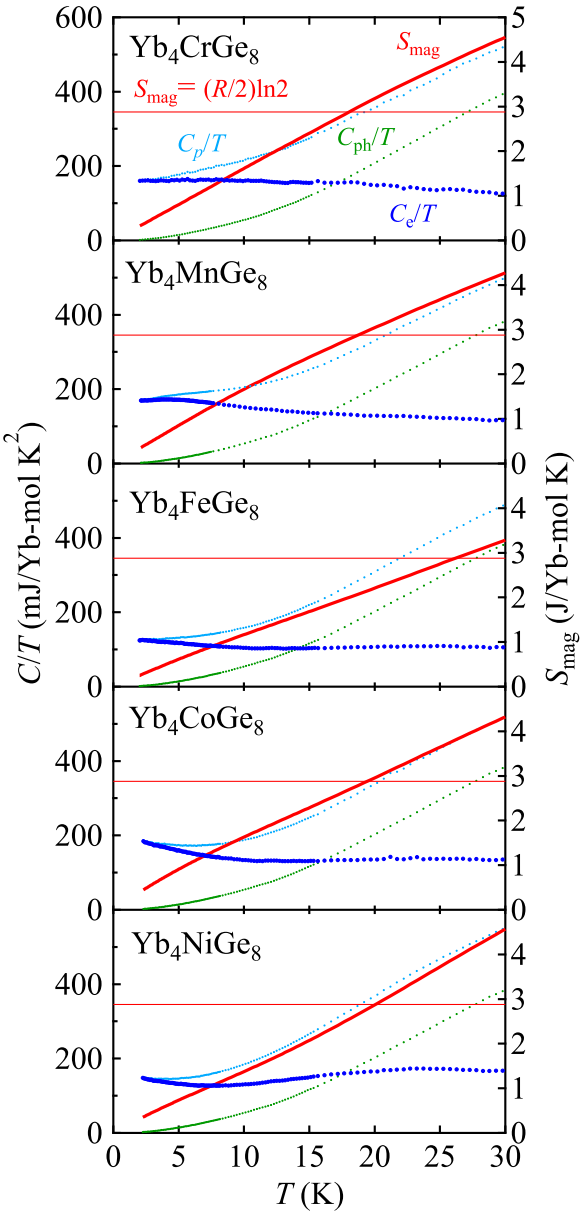

FIG. 7. Temperature dependence of the electronic heat capacity divided by temperature C_e/T (left axis) and the magnetic entropy S_{mag} (right axis) in Yb_4TGe_8 (T = Cr, Mn, Fe, Co, and Ni) below 30 K, where C_e/T is obtained by subtracting the phonon contribution C_{ph} from the heat capacity C_p. The horizontal line shows $S_{mag} = (R/2)\ln 2$.

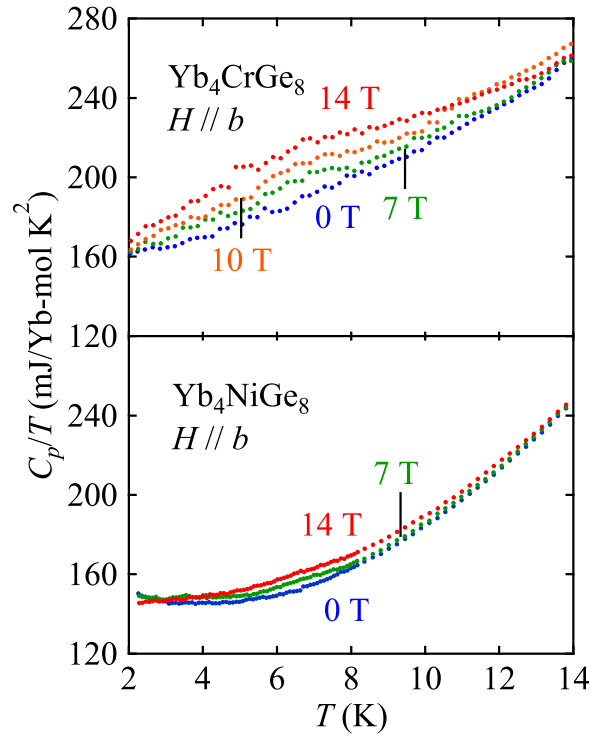

FIG. 8. Temperature dependence of the heat capacity divided by temperature C_p/T in Yb_4CrGe_8 and Yb_4NiGe_8 below 14 K under several magnetic fields H for $H \parallel b$.

remains in Yb_4FeGe_8, Yb_4CoGe_8, and Yb_4NiGe_8. A broad peak around 23 K in Yb_4NiGe_8 would be attributed to the Kondo effect, and a slight broad peak is observed around similar temperature in Yb_4FeGe_8 and Yb_4CoGe_8. In the cases of Yb_4CrGe_8 and Yb_4MnGe_8, the above-mentioned upturn of C_e/T which occurs at higher temperatures may lead masking of a peak behavior of C_e/T. It is expected that the carrier density in Yb_4TGe_8 depends on the $3d$-orbital filling in T atoms within the rigid-band model. The temperature region, in which the additional magnetic correlation affects C_e/T, systematically shifts to lower temperatures with increasing the number of electrons in T atom as mentioned above. Therefore, the band filling would have a significant effect on the anomalous low-temperature physical properties.

The magnetic entropy S_{mag} can be roughly estimated from the integration of C_e/T. Figure 7 shows the temperature dependence of S_{mag}. The horizontal line in Fig. 7 shows $S_{mag} = (R/2)\ln 2$, and the temperature at which S_{mag} reaches $(R/2)\ln 2$, $T_{S_{mag}}$, could be regarded as roughly half of T_K. The values of $2T_{S_{mag}}$ for Yb_4TGe_8 (T = Cr, Mn, Fe, Co, and Ni) are 35, 37, 53, 39, and 40 K, respectively. These values are close to T_χ^{max}, and there is little difference among the five compounds.

Figure 8 shows the temperature dependence of C_p/T in Yb_4CrGe_8 and Yb_4NiGe_8 below 10 K under several magnetic fields. The results of Yb_4MnGe_8, Yb_4FeGe_8, and Yb_4CoGe_8 are shown in the Supplemental Material [52]. For all five compounds, C_p/T tends to increase with increasing magnetic field. The phonon contribution to C_p/T does not change significantly with increasing magnetic field. An extra contribution induced by the magnetic field would be added to C_p/T. In addition, the low-temperature upturn of C_p/T in Yb_4CoGe_8 and Yb_4NiGe_8 under zero magnetic field is suppressed with increasing magnetic field. The origin of these behaviors will be discussed later.

D. Electrical resistivity

The insets in Fig. 9 show the temperature dependence of the electrical resistivity ρ in Yb_4TGe_8 (T = Cr, Mn, Fe, Co, and Ni) between 2 and 300 K under zero magnetic field with the current applied parallel to the a axis. In all the five compounds, ρ increases with increasing temperature, suggesting

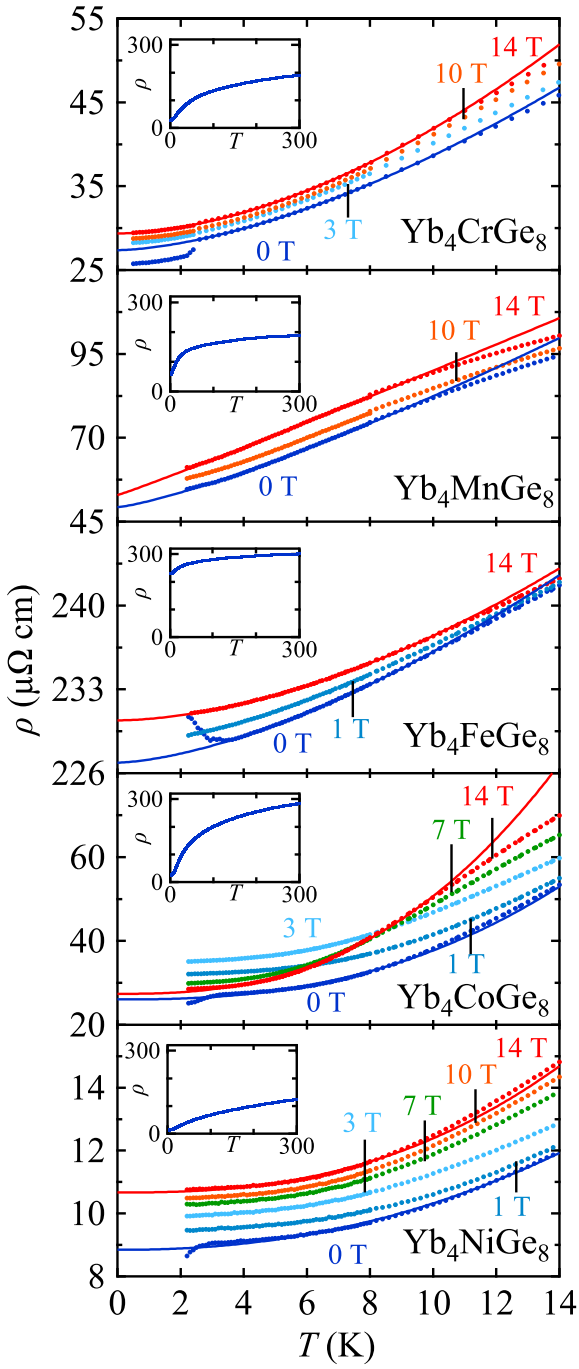

FIG. 9. Temperature dependence of electrical resistivity ρ in Yb_4TGe_8 (T = Cr, Mn, Fe, Co, and Ni) under several magnetic fields H for $H \parallel b$ with the current parallel to the a axis. The solid lines show the fit with the function $\rho = \rho_0 + AT^n$ to the data under $\mu_0 H = 0$ and 14 T below 10 K. The insets show the temperature dependence of ρ between 2 and 300 K.

the metallic properties. No anomaly indicating magnetic ordering appears, and this is consistent with the behavior of the temperature dependence of M/H and C_p/T. The slope of the $\rho - T$ curves of the five compounds becomes steeper at low temperatures. This suggests a crossover from the single-ion Kondo regime to the Kondo-lattice state. At even lower temperatures, the additional magnetic correlation develops and would fluctuate spatially and/or temporally in the Kondo-lattice state.

TABLE IV. Values of ρ_0, A, and n estimated from data fit using the function $\rho = \rho_0 + AT^n$ below 10 K under $\mu_0 H = 0$ and 14 T. The numbers in parentheses are the standard deviations in the last significant figures.

T	$\mu_0 H$ (T)	ρ_0 ($\mu\Omega$ cm)	A ($\mu\Omega$ cm/K^n)	n
Cr	0	27.37(4)	0.280(10)	1.60(1)
	14	29.36(8)	0.221(8)	1.75(2)
Mn	0	49.3(4)	1.9(2)	1.25(3)
	14	52.9(6)	3.4(3)	1.05(3)
Fe	0	226.88(5)	0.254(10)	1.56(2)
	14	230.41(2)	0.128(4)	1.74(1)
Co	0	26.0(3)	0.04(1)	2.48(14)
	14	27.4(2)	0.07(1)	2.55(7)
Ni	0	8.84(4)	0.011(2)	2.19(8)
	14	10.67(3)	0.005(2)	2.52(13)

Figure 9 shows the temperature dependence of ρ in Yb_4TGe_8 (T = Cr, Mn, Fe, Co, and Ni) under several magnetic fields for $H \parallel b$ with the current applied parallel to the a axis. In Yb_4CrGe_8, Yb_4CoGe_8, and Yb_4NiGe_8, ρ decreases drastically below 3.4 K. This is due to an extrinsic superconductivity of the indium flux [53], which could not be completely removed from the surface of the single crystal. In Yb_4FeGe_8, ρ increases rapidly below 3 K. This is possibly due to the weak localization [54] caused by the small imperfection of the single crystal and the low dimensionality of the crystal structure. Indeed, peaks in powder XRD spectrum of Yb_4FeGe_8 are broader than those of the other compounds as shown in Fig. 1. The rapid increase of ρ is suppressed under the magnetic field of 1 T. This is a proof of contributions of the additional magnetic correlation to the weak localization.

All the five compounds exhibit a positive magnetoresistance below 14 K, while a negative magnetoresistance appears below 8.8 K in Yb_4CoGe_8. The spins on the Yb^{3+} ions induced by the destruction of the Kondo singlet state cannot be easily oriented along to the magnetic field direction possibly due to the magnetic anisotropy. Magnetizations of the five compounds are $\sim 0.3\,\mu_B$ under the magnetic field of 14 T as shown in the Supplemental Material [52]. In addition, the additional magnetic correlation is easily destabilized by the magnetic field. Therefore, the destabilization of the Kondo-lattice state would cause a positive magnetoresistance like the paramagnetic state, and the suppression of the additional magnetic correlation would cause a negative magnetoresistance.

The solid lines show the fit of the ρ data under $\mu_0 H = 0$ and 14 T below 10 K using the power law, $\rho = \rho_0 + AT^n$, where ρ_0 is the residual resistivity, A is the contribution of scattering between conduction electrons to ρ, and n is a power index. The data of ρ under zero magnetic field in Yb_4CrGe_8, Yb_4CoGe_8, and Yb_4NiGe_8 below 3.4 K and in Yb_4FeGe_8 below 3 K are excluded from the fit range. The values of ρ_0, A, and n estimated from the fit are listed in Table IV. The value of ρ_0 is significantly different for each compound. This reflects the difference in degree of imperfection in single crystals. The value of n is smaller than 2 in Yb_4CrGe_8, Yb_4MnGe_8, and Yb_4FeGe_8 and is larger than 2 in Yb_4CoGe_8

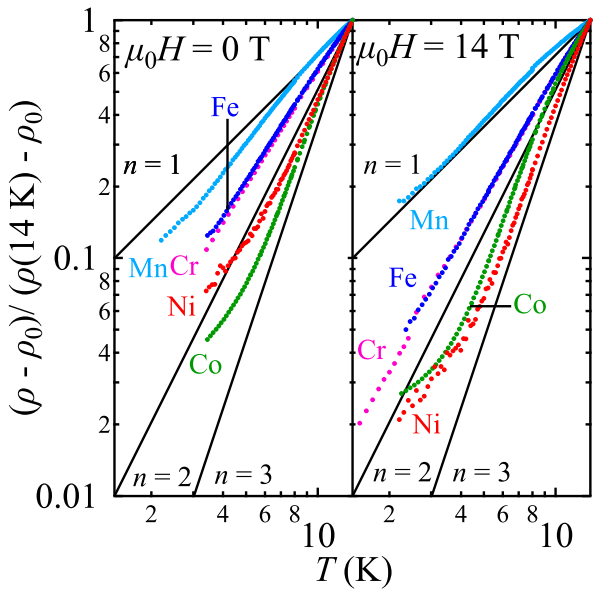

FIG. 10. Plot of $\log\{(\rho - \rho_0)/[\rho(14\,\text{K}) - \rho_0]\}$ vs $\log T$ for Yb_4TGe_8 (T = Cr, Mn, Fe, Co, and Ni) below 14 K under μH = 0 and 14 K.

and Yb_4NiGe_8, suggesting that all the five compounds are not of a simple FL. In addition, the application of the magnetic field of 14 T increases n in Yb_4CrGe_8 and Yb_4FeGe_8 and decreases n in Yb_4MnGe_8, Yb_4CoGe_8, and Yb_4NiGe_8. To confirm validity of estimation in n, a modified resistivity $(\rho - \rho_0)/[\rho(14\text{ K}) - \rho_0]$ is plotted against temperature on a double-logarithmic scale, as shown in Fig. 10. The slope of the double-logarithmic graph corresponds to n. This plot highly depends on ρ_0 estimated form the fit of ρ data in Fig. 9. In Yb_4CrGe_8 and Yb_4FeGe_8, n takes constant value under both conditions of $\mu_0H = 0$ and 14 T. On the other hand, n in Yb_4MnGe_8, Yb_4CoGe_8, and Yb_4NiGe_8 changes in a small temperature range. This suggests that the contribution of the additional magnetic correlation to ρ is large. The behavior of ρ in Yb_4MnGe_8, Yb_4CoGe_8, and Yb_4NiGe_8 could not be explained by a simple fluid model with a constant power index at low temperatures. Therefore, the standard deviation of A in Yb_4MnGe_8, Yb_4CoGe_8, and Yb_4NiGe_8 is large as shown in Table IV.

IV. DISCUSSION

We have presented the physical properties of Yb_4TGe_8 (T = Cr, Mn, Fe, Co, and Ni). All the five compounds exhibit typical behaviors for Kondo-lattice system above 10 K, while the additional magnetic correlation develops at low temperatures. Here, we discuss the origin of the anomalous behavior at low temperatures.

First, we consider the Kondo disorder [55] or the Kondo hole effect [56], which is caused by the Yb lattice vacancy. To confirm the lattice imperfection, the residual resistivity ratio RRR = ρ(300 K)/ρ(4.2 K) is estimated. The value of RRR for Yb_4TGe_8 (T = Cr, Mn, Fe, Co, and Ni) is 6.3, 3.0, 1.3, 10.3, and 9.3, respectively. The low-temperature enhancement of M/H and C_p/T in Yb_4CoGe_8 and Yb_4NiGe_8 is more remarkable than that of Yb_4CrGe_8, Yb_4MnGe_8, and Yb_4FeGe_8 as shown before. On the other hand, RRR in Yb_4CoGe_8 and Yb_4NiGe_8 is larger than that of Yb_4CrGe_8, Yb_4MnGe_8, and Yb_4FeGe_8, suggesting that the Yb lattice vacancies of Yb_4CoGe_8 and Yb_4NiGe_8 are possibly less than those of Yb_4CrGe_8, Yb_4MnGe_8, and Yb_4FeGe_8. Therefore, the Kondo disorder or the Kondo hole effect cannot be the origin of the anomalous behavior at low temperatures. Rather, the origin could be an additional magnetic correlation, which has often been discussed in intermediate valence systems. The present system belongs to the intermediate valence system [46,47], and the low-temperature anomalies for Yb_4TGe_8 (T = Cr, Mn, Fe, Co, and Ni) could be discussed in this scheme.

We focus on several intermediate valence compounds that exhibit additional magnetic correlations at low temperatures similar to Yb_4TGe_8. One example is $YbAl_3$, in which χ reaches a maximum at approximately 120 K and is enhanced below 45 K [57]. Since the measurement was performed using single crystals pure enough to exhibit de Haas–van Alphen signals, the behavior is intrinsic and not due to the impurity effect. Similar phenomena are also observed in $CePd_3$, in which χ reaches a maximum at approximately 130 K, and an additional magnetic correlation develops below 50 K [58]. Inelastic neutron scattering experiments reveal the growth of low-energy fluctuations at low temperatures [59]. In addition, the pronounced Q dependence exhibited in the inelastic neutron scattering spectrum at 7 K suggests that the coherent effect is enhanced at low temperatures [60]. Furthermore, the magnetic form factor estimated from polarized neutron scattering implies that the hybridization between the $4f$ and $5d$ orbitals of Ce^{3+} ions is promoted at low temperatures [61]. Thus, the additional magnetic correlation also develops in several other ytterbium- and cerium-based compounds. On the other hand, it is reported that the energy of x-ray absorption near-edge structure spectra of Mn edge at 20 K in Yb_4MnGe_8 is higher than that at room temperature [47]. In our previous paper as well, the energy of x-ray absorption spectra of Cr edge in Yb_4CrGe_8 is higher at low temperatures [46]. These facts imply the strong relation between $3d$ electron carriers and the additional magnetic correlation in the present case of Yb_4TGe_8. It is highlighted that a quasi-kagome-lattice compound CeIrSn with $T_K \sim 480$ K displays additional magnetic correlations [62]. This compound exhibits anomalous negative in-plane thermal expansion below 2 K and negative volume magnetostriction below approximately 5 T under the condition of the magnetic field applying to the a axis. It is proposed that these behaviors are caused by the competition between Kondo singlet formation and antiferromagnetic correlation resulting from geometrical frustration. The presence of additional magnetic correlations is discussed not only in the intermediate valence system, but also in the heavy-fermion system such as $Ce_{1-x}La_xCoIn_5$, suggesting that the screening of the magnetic moments involves antiferromagnetic intersite correlations by the neighboring localized moments [63].

Next, we discuss the origin of the difference in physical properties of the five compounds at low temperatures. The temperature dependence of the Yb valence in Yb_4CrGe_8 and Yb_4MnGe_8 has been found to differ below 150 K [46], suggesting that the strength of hybridization between conduction electrons and $4f$ electrons, so-called $c - f$ hybridization,

changes depending on T atoms. The chemical pressure affects the strength of $c-f$ hybridization. Since the ionic radius of the Yb^{3+} ion is smaller than that of the Yb^{2+} ion, the effect of $c-f$ hybridization is weakened as the unit cell shrinks. As a result, a different behavior from FL can be expected near the magnetic QCP. The unit-cell volume of Yb_4NiGe_8 is the largest among the five compounds. Therefore, the distance from the magnetic QCP is the largest for Yb_4NiGe_8, and the low-temperature behavior of Yb_4NiGe_8 would have FL characters. However, as shown in Figs. 5 and 6, M/H and C_p/T in Yb_4NiGe_8 are enhanced more than those of Yb_4CrGe_8, Yb_4MnGe_8, and Yb_4FeGe_8. This suggests that low-temperature physical properties in the five compounds cannot be explained solely by $c-f$ hybridization effect. In addition, the values of $T_\chi^{\max}$ and $2T_{S_{\rm mag}}$ as a guide for $T_{\rm K}$ have approximately the same value of the five compounds. If the positive chemical pressure effectively weakened $c-f$ hybridization, the value of $T_\chi^{\max}$ and $2T_{S_{\rm mag}}$ should decrease more drastically with shrinking the unit cell. Further, the value of γ in Yb_4TGe_8 (T = Cr, Mn, Fe, Co, and Ni) is also smaller than 210–460 ($\rm mJ/mol\,K^2$) in a typical Kondo-lattice compound $YbCu_{5-x}Ag_x$ ($0.12\leqslant x\leqslant 1.0$) [17], even if the enhancement at low temperatures is taken into consideration. If the distance from the magnetic QCP was the main factor of the differences in physical properties in Yb_4TGe_8 (T = Cr, Mn, Fe, Co, and Ni) at low temperatures, then the value of γ should be much larger. Therefore, the change of $c-f$ hybridization through the chemical pressure effect is not the main reason for the difference in the low-temperature physical properties of the five compounds.

To clarify the role of T atoms in Yb_4TGe_8 in more detail, we take the physical properties of Y_4TGe_8 into account, in which Yb atoms in Yb_4TGe_8 are replaced with nonmagnetic Y atoms. It is reported that $YCr_{0.22}Ge_2$, $YFe_{0.282}Ge_2$, and $YCo_{0.493}Ge_2$ exhibit the Pauli paramagnetic behavior [64]. We also succeed in growing a single crystal of Y_4MnGe_8 and have revealed that this compound exhibits the enhanced Pauli paramagnetic behavior [52]. In addition, the value of $\mu_{\rm eff}$ in Yb_4TGe_8 roughly agrees with the theoretical value for the free Yb^{3+} ion, as mentioned previously. Therefore, $3d$ electrons in T atoms would behave itinerantly in Yb_4TGe_8 (T = Cr, Mn, Fe, Co, and Ni) and change the carrier density depending on the number of electrons in T atoms. In the intermediate valence compounds $YbXCu_4$ (X = Ag, Cd, In, Mg, Tl, and Zn), the carrier density is a dominant factor to determine the magnetic state [65]. The crossover from the low-temperature FL state to the high-temperature paramagnetic state of $YbXCu_4$ is slow due to so-called protracted screening [66]. Since protracted screening highly depends on the carrier density, physical properties of $YbXCu_4$ (X = Ag, Cd, In, Mg, Tl, and Zn) change depending on the X atoms. In the present case as well, the change of T atom results in different band fillings within the framework of the rigid band model. The change of the carrier density would lead a complicated many-body effect, resulting in an unconventional phenomenon such as an additional magnetic correlation.

Finally, we will discuss the origin of C_p/T behavior in Yb_4TGe_8 (T = Cr, Mn, Fe, Co, and Ni) under the magnetic field. In the itinerant compounds $CeSn_3$ [67] and Sc_3In [68], the $C_p/T-T$ curves under the magnetic field behave similarly to the present case. It is proposed that coefficient of the T^2 term in the C_p/T-T increases due to the development of the induced magnetic moment on Ce or Sc atoms, and the low-temperature upturn in the C_p/T-T suppresses due to the suppression of spin fluctuation. In $CeSn_3$, the anisotropy of the suppression of spin fluctuations is also reported [69]. In the present case, C_p/T is enhanced by the magnetic field. This would result from the shift in entropy from above 14 K into the displayed temperature range due to the decrease in $T_{\rm K}$ with increasing magnetic field. The low-temperature upturn in the C_p/T-T observed in Yb_4CoGe_8 and Yb_4NiGe_8 is suppressed by the magnetic field. This is possibly due to suppression of the additional magnetic correlation. In the present stage, it is unclear whether the additional magnetic correlation occurs in another band and coexists with the Kondo-lattice state or completely destroys the Kondo-lattice state. The details must be clarified in the future.

V. CONCLUSIONS

The magnetic, thermal, and transport properties of Yb_4TGe_8 (T = Cr, Mn, Fe, Co, and Ni) were studied using their single crystals. All the compounds exhibit conventional physical properties for the Kondo-lattice system at high temperatures. In contrast, the additional magnetic correlation develops at low temperatures with different extent in each compound. Such an unconventional additional magnetic correlation would arise from the complicated many-body effect and highly depends on the carrier density which changes with the variation of T atoms. Further studies are required on ytterbium-based compounds containing a $3d$ transition element.

ACKNOWLEDGMENTS

This work was supported by JSPS KAKENHI Grant No. JP18KK0150. Part of this work was performed at the institute for Solid State Physics at University of Tokyo.

[1] M. A. Ruderman and C. Kittel, Indirect exchange coupling of nuclear magnetic moments by conduction electrons, Phys. Rev. **96**, 99 (1954).

[2] T. Kasuya, A theory of metallic ferro- and antiferromagnetism on Zener's model, Prog. Theor. Phys. **16**, 45 (1956).

[3] K. Yosida, Magnetic properties of Cu-Mn alloys, Phys. Rev. **106**, 893 (1957).

[4] J. Kondo, Resistance minimum in dilute magnetic alloys, Prog. Theor. Phys. **32**, 37 (1964).

[5] A. A. Abrikosov, Electron scattering on magnetic impurities in metals and anomalous resistivity effects, Physics **2**, 5 (1965).

[6] Y. Nagaoka, Self-consistent treatment of Kondo's effect in dilute alloys, Phys. Rev. **138**, A1112 (1965).

[7] A. Sumiyama, Y. Oda, H. Nagano, Y. Ōnuki, K. Shibutani, and T. Komatsubara, Coherent Kondo state in a dense Kondo substance: $Ce_xLa_{1-x}Cu_6$, J. Phys. Soc. Jpn. **55**, 1294 (1986).

[8] S. Doniach, The Kondo lattice and weak antiferromagnetism, Physica B+C **91**, 231 (1977).

[9] T. Takeuchi, A. Thamizhavel, T. Okubo, M. Yamada, N. Nakamura, T. Yamamoto, Y. Inada, K. Sugiyama, A. Galatanu, E. Yamamoto, K. Kindo, T. Ebihara, and Y. Ōnuki, Anisotropic, thermal, and magnetic properties of $CeAgSb_2$: Explanation via a crystalline electric field scheme, Phys. Rev. B **67**, 064403 (2003).

[10] A. Thamizhavel, T. Takeuchi, T. Okubo, M. Yamada, R. Asai, S. Kirita, A. Galatanu, E. Yamamoto, T. Ebihara, Y. Inada, R. Settai, and Y. Ōnuki, Anisotropic electrical and magnetic properties of $CeTSb_2$ (T = Cu, Au, and Ni) single crystals, Phys. Rev. B **68**, 054427 (2003).

[11] R. Mondal, R. Bapat, S. K. Dhar, and A. Thamizhavel, Magnetocrystalline anisotropy in the Kondo-lattice compound $CeAgAs_2$, Phys. Rev. B **98**, 115160 (2018).

[12] J. Lee, A. Rabus, N. R. Lee-Hone, D. M. Broun, and E. Mun, The two-dimensional metallic triangular lattice antiferromagnet $CeCd_3P_3$, Phys. Rev. B **99**, 245159 (2019).

[13] L. Wang, C. Wang, Z. Liu, J. Cheng, S. Miao, Y. Song, Y. Shi, and Y. Yang, Magnetic phase diagrams of the ferromagnetic Kondo lattice $CePd_2Al_8$, Phys. Rev. B **100**, 085122 (2019).

[14] T. Mazet, H. Ihou-Mouko, D. H. Ryan, C. J. Voyer, J. M. Cadogan, and B. Malaman, Valence change and magnetic order in $YbMn_6Ge_{6-x}Sn_x$, J. Phys.: Condens. Matter **22**, 116005 (2010).

[15] I. R. Fisher, T. A. Wiener, S. L. Bud'ko, P. C. Canfield, J. Y. Chan, and S. M. Kauzlarich, Thermodynamic and transport properties of single-crystal $Yb_{14}MnSb_{11}$, Phys. Rev. B **59**, 13829 (1999).

[16] A. Generalov, D. A. Sokolov, A. Chikina, Y. Kucherenko, V. N. Antonov, L. V. Bekenov, S. Patil, A. D. Huxley, J. W. Allen, K. Matho, K. Kummer, D. V. Vyalikh, and C. Laubschat, Insight into the temperature dependent properties of the ferromagnetic Kondo lattice YbNiSn, Phys. Rev. B **95**, 184433 (2017).

[17] N. Tsujii, J. He, K. Yoshimura, K. Kosuge, H. Michor, K. Kreiner, and G. Hilscher, Heavy-fermion behavior in $YbCu_{5-x}Ag_x$s, Phys. Rev. B **55**, 1032 (1997).

[18] N. Tsujii, K. Yoshimura, and K. Kosuge, Cu nuclear quadrupole resonance and relaxation on the Yb-based heavy-fermion compound $YbCu_5$, Phys. Rev. B **59**, 11813 (1999).

[19] N. Tsujii, J. He, F. Amita, K. Yoshimura, K. Kosuge, H. Michor, G. Hilscher, and T. Goto, Kondo-lattice formation in cubic-phase $YbCu_5$, Phys. Rev. B **56**, 8103 (1997).

[20] A. Miyake, Y. Sato, M. Tokunaga, J. Jatmika, and T. Ebihara, Different metamagnetism between paramagnetic Ce and Yb isomorphs, Phys. Rev. B **96**, 085127 (2017).

[21] Y. Ōnuki, Y. Shimizu, and T. Komatsubara, Magnetic property of a new Kondo lattice intermetallic compound: $CeCu_6$, J. Phys. Soc. Jpn. **53**, 1210 (1984).

[22] Y. Ōnuki, Y. Shimizu, and T. Komatsubara, Anisotropic magnetic property of Kondo lattice substance: $CeCu_6$, J. Phys. Soc. Jpn. **54**, 304 (1985).

[23] W. Zhou, C. Q. Xu, B. Li, R. Sankar, F. M. Zhang, B. Qian, C. Cao, J. H. Dai, J. Lu, W. X. Jiang, D. Qian, and X. Xu, Kondo behavior and metamagnetic phase transition in the heavy-fermion compound $CeBi_2$, Phys. Rev. B **97**, 195120 (2018).

[24] J. G. Sereni, I. Čurlík, M. Giovannini, A. Strydom, and M. Reiffers, Physical properties of the magnetically frustrated very-heavy-fermion compound $YbCu_4Ni$, Phys. Rev. B **98**, 094420 (2018).

[25] Y. Ōnuki, S. Yasui, M. Matsushita, S. Yoshiuchi, M. Ohya, Y. Hirose, N. D. Dung, F. Honda, T. Takeuchi, R. Settai, K. Sugiyama, E. Yamamoto, T. D. Matsuda, Y. Haga, T. Tanaka, Y. Kubo, and H. Harima, Characteristic heavy fermion properties in $YbCu_2Si_2$ and YbT_2Zn_{20} (T: Co, Rh, Ir), J. Phys. Soc. Jpn. **80**, SA003 (2011).

[26] T. Yamashita, R. Miyazaki, Y. Aoki, and S. Ohara, Transport, thermal, and magnetic properties of $YbNi_3X_9$ (X = Al, Ga): A newly synthesized Yb-based Kondo lattice system, J. Phys. Soc. Jpn. **81**, 034705 (2012).

[27] Y. P. Singh, R. B. Adhikari, D. J. Haney, B. D. White, M. B. Maple, M. Dzero, and C. C. Almasan, Zero-field quantum critical point in $Ce_{0.91}Yb_{0.09}CoIn_5$, Phys. Rev. B **97**, 184514 (2018).

[28] S. Pandey, V. Siruguri, and R. Rawat, Quantum critical point and intermediate valence fluctuations in $CeRu_{2-x}Co_xGe_2$, Phys. Rev. B **98**, 155129 (2018).

[29] E. Bauer, R. Hauser, A. Galatanu, H. Michor, G. Hilscher, J. Sereni, M. G. Berisso, P. Pedrazzini, M. Galli, F. Marabelli, and P. Bonville, Non-Fermi-liquid behavior of $YbCu_{5-x}Al_x$, Phys. Rev. B **60**, 1238 (1999).

[30] F. Steglich, P. Hellman, S. Thomas, P. Gegenwart, A. Link, R. Helfrich, G. Sparn, M. Lang, C. Geibel, and W. Assmus, "Non-Fermi-liquid" phenomena in heavy-fermion $CeCu_2Si_2$ and $CeNi_2Ge_2$, Physica B: Condens. Matter **237-238**, 192 (1997).

[31] A. Neubert, T. Pietrus, O. Stockert, H. V. Löhneysen, A. Rosch, and P. Wölfle, Electrical resistivity of the non-Fermi-liquid alloy $CeCu_{5.9}Au_{0.1}$, Physica B: Condens. Matter **230-232**, 587 (1997).

[32] F. Steglich, H. Pfau, S. Lausberg, S. Hamann, P. Sun, U. Stockert, M. Brando, S. Friedemann, C. Krellner, C. Geibel, S. Wirth, S. Kirchner, E. Abrahams, and Q. Si, Evidence of a Kondo destroying quantum critical point in $YbRh_2Si_2$, J. Phys. Soc. Jpn. **83**, 061001 (2014).

[33] F. Steglich, J. Aarts, C. D. Bredl, W. Lieke, D. Meschede, W. Franz, and H. Schäfer, Superconductivity in the Presence of Strong Pauli Paramagnetism: $CeCu_2Si_2$, Phys. Rev. Lett. **43**, 1892 (1979).

[34] N. Pouse, S. Jang, B. D. White, S. Ran, R. B. Adhikari, C. C. Almasan, and M. B. Maple, Temperature versus Sm concentration phase diagram and quantum criticality in the correlated electron system $Ce_{1-x}Sm_xCoIn_5$, Phys. Rev. B **97**, 235149 (2018).

[35] V. S. Zapf, E. J. Freeman, E. D. Bauer, J. Petricka, C. Sirvent, N. A. Frederick, R. P. Dickey, and M. B. Maple, Coexistence of superconductivity and antiferromagnetism in $CeRh_{1-x}Co_xIn_5$, Phys. Rev. B **65**, 014506 (2001).

[36] N. D. Mathur, F. M. Grosche, S. R. Julian, I. R. Walker, D. M. Freye, R. K. W. Haselwimmer, and G. G. Lonzarich, Magnetically mediated superconductivity in heavy fermion compounds, Nature (London) **394**, 39 (1998).

[37] H. Hegger, C. Petrovic, E. G. Moshopoulou, M. F. Hundley, J. L. Sarrao, Z. Fisk, and J. D. Thompson, Pressure-Induced Superconductivity in Quasi-2D $CeRhIn_5$, Phys. Rev. Lett. **84**, 4986 (2000).

[38] K. Yoshimura, T. Nitta, M. Mekata, T. Shimizu, T. Sakakibara, T. Goto, and G. Kido, Anomalous High-Field Magnetization and Negative Forced Volume Magnetostriction in $Yb_{1-x}M_xCu_2$ (M = InandAg)-Evidence for Valence Change in High Magnetic Fields, Phys. Rev. Lett. **60**, 851 (1988).

[39] T. Shimizu, K. Yoshimura, T. Nitta, T. Sakakibara, T. Goto, and M. Mekata, Temperature- and field-induced valence change in $Yb_xIn_{1-x}Cu_2$, J. Phys. Soc. Jpn. **57**, 405 (1988).

[40] S. Yamanaka, T. Nakahigashi, C. Michioka, H. Ueda, A. Matsuo, K. Kindo, and K. Yoshimura, Synthesis and physical properties of $Yb_{1+x}In_{1-x}Cu_4$ -two-step magnetic anomaly in the high field magnetization process-, J. Jpn. Soc. Powder Powder Metallurgy **67**, 84 (2020).

[41] T. Mazet, D. Malterre, M. Francois, C. Dallera, M. Grioni, and G. Monaco, Nonpareil Yb Behavior in $YbMn_6Ge_{6-x}Sn_x$, Phys. Rev. Lett. **111**, 096402 (2013).

[42] T. Mazet, D. Malterre, M. Francois, L. Eichenberger, M. Grioni, C. Dallera, and G. Monaco, Composition and temperature dependence of the Yb valence in $YbMn_6Ge_{6-x}Sn_x$ studied by RIXS, Phys. Rev. B **92**, 075105 (2015).

[43] H. Yamaoka, I. Jarrige, N. Tsujii, J. Lin, N. Hiraoka, H. Ishii, and K. Tsuei, Temperature and pressure-induced valence transitions in $YbNi_2Ge_2$ and $YbPd_2Si_2$, Phys. Rev. B **82**, 035111 (2010).

[44] H. Yamaoka, N. Tsujii, Y. Utsumi, H. Sato, I. Jarrige, Y. Yamamoto, J. Lin, N. Hiraoka, H. Ishii, K. Tsuei, and J. Mizuki, Valence transitions in the heavy-fermion compound YbCuAl as a function of temperature and pressure, Phys. Rev. B **87**, 205120 (2013).

[45] H. Yamaoka, N. Tsujii, Y. Yamamoto, Y. Michiue, J. Lin, N. Hiraoka, H. Ishii, K. Tsuei, and J. Mizuki, Reentrant valence transition in $YbCu_{4.5}$ under pressure, Phys. Rev. B **97**, 085106 (2018).

[46] H. Yamaoka, S. Yamanaka, M. Hikiji, C. Michioka, N. Tsujii, H. Sato, K. Shimada, N. Hiraoka, H. Ishii, and K. Yoshimura, Temperature and pressure dependence of the electronic and crystal structure of Yb_4TGe_8 (T = Cr, Mn, Fe, Co, and Ni) studied by high-resolution x-ray absorption spectroscopy, x-ray diffraction, and photoelectron spectroscopy, J. Phys. Soc. Jpn. **91**, 024704 (2022).

[47] S. C. Peter, M. Chondroudi, C. D. Malliakas, M. Balasubramanian, and M. G. Kanatzidis, Anomalous thermal expansion in the square-net compounds RE_4TGe_8 (RE = Yb, Gd; T = Cr-Ni, Ag), J. Am. Chem. Soc. **133**, 13840 (2011).

[48] W. Kraus and G. Nolze, POWDER CELL - a program for the representation and manipulation of crystal structures and calculation of the resulting x-ray powder patterns, J. Appl. Cryst. **29**, 301 (1996).

[49] F. L. Faita, K. Ersching, J. J. S. Acuña, C. E. M. Campos, and P. S. Pizani, Structure and microstructure of In_4Te_3 nanopowders prepared by solid state reaction, Mater. Chem. Phys. **130**, 1361 (2011).

[50] H. Bie, A. V. Tkachuk, and A. Mar, Structure and magnetic properties of rare-earth chromium germanides $RECr_xGe_2$ (RE = Sm, Gd-Er), J. Solid State Chem. **182**, 122 (2009).

[51] S. C. Peter, S. Rayaprol, M. C. Francisco, and M. G. Kanatzidis, Crystal structure and properties of $Yb_5Ni_4Ge_{10}$, Eur. J. Inorg. Chem. **2011**, 3963 (2011).

[52] See Supplemental Material at http://link.aps.org/supplemental/10.1103/PhysRevB.106.024402 for the temperature dependence of the magnetic susceptibility in Y_4MnGe_8, the magnetization process in Yb_4TGe_8 (T = Cr, Mn, Fe, Co, and Ni), and the temperature dependence of the heat capacity divided by temperature under several magnetic fields in Yb_4TGe_8 (T = Mn, Fe, and Co).

[53] M. P. Conley and R. W. Reed, Ultrasonic attenuation in normal and superconducting indium, J. Low Temp. Phys. **43**, 461 (1981).

[54] E. Abrahams, P. W. Anderson, D. C. Licciardello, and T. V. Ramakrishnan, Scaling Theory of Localization: Absence of Quantum Diffusion in Two Dimensions, Phys. Rev. Lett. **42**, 673 (1979).

[55] O. O. Bernal, D. E. MacLaughlin, A. Amato, R. Feyerherm, F. N. Gygax, A. Schenck, R. H. Heffner, L. P. Le, G. J. Nieuwenhuys, B. Andraka, H. V. Löhneysen, O. Stockert, and H. R. Ott, Kondo disorder and non-Fermi-liquid behavior in $UCu_{5-x}Pd_x$ and $CeCu_{5.9}Au_{0.1}$, Phys. Rev. B **54**, 13000 (1996).

[56] J. M. Lawrence, T. Graf, M. F. Hundley, D. Mandrus, J. D. Thompson, A. Lacerda, M. S. Torikachvili, J. L. Sarrao, and Z. Fisk, Kondo hole behavior in $Ce_{0.97}La_{0.03}Pd_3$, Phys. Rev. B **53**, 12559 (1996).

[57] A. L. Cornelius, J. M. Lawrence, T. Ebihara, P. S. Riseborough, C. H. Booth, M. F. Hundley, P. G. Pagliuso, J. L. Sarrao, J. D. Thompson, M. H. Jung, A. H. Lacerda, and G. H. Kwei, Two Energy Scales and Slow Crossover in $YbAl_3$, Phys. Rev. Lett. **88**, 117201 (2002).

[58] J. Aarts, F. R. de Boer, P. F. de Châtel, and A. Menovsky, The magnetic behaviour of $CePd_3$ at low temperatures, Solid State Commun. **56**, 623 (1985).

[59] S. M. Shapiro, C. Stassis, and G. Aeppli, Spin-Fluctuation Spectra Measured on a Single Crystal of $CePd_3$, Phys. Rev. Lett. **62**, 94 (1989).

[60] V. R. Fanelli, J. M. Lawrence, E. A. Goremychkin, R. Osborn, E. D. Bauer, K. J. McClellan, J. D. Thompson, C. H. Booth, A. D. Christianson, and P. S. Riseborough, Q-dependence of the spin fluctuations in the intermediate valence compound $CePd_3$, J. Phys.: Condens. Matter **26**, 225602 (2014).

[61] C. Stassis, C. K. Loong, J. Zarestky, O. D. McMasters, R. M. Moon, and J. R. Thompson, Temperature dependence of the field induced magnetic form factor of the intermediate valence compound $CePd_3$, J. Appl. Phys. **53**, 7890 (1982).

[62] Y. Shimura, A. Wörl, M. Sundermann, S. Tsuda, D. T. Adroja, A. Bhattacharyya, A. M. Strydom, A. D. Hillier, F. L. Pratt, A. Gloskovskii, A. Severing, T. Onimaru, P. Gegenwart, and T. Takabatake, Antiferromagnetic Correlations in Strongly Valence Fluctuating CeIrSn, Phys. Rev. Lett. **126**, 217202 (2021).

[63] S. Nakatsuji, S. Yeo, L. Balicas, Z. Fisk, P. Schlottmann, P. G. Pagliuso, N. O. Moreno, J. L. Sarrao, and J. D. Thompson,

Intersite Coupling Effects in a Kondo Lattice, Phys. Rev. Lett. **89**, 106402 (2002).

[64] L. Gustin, L. Xing, M. T. Pan, R. Jin, and W. Xie, Electron counts, structural stability, and magnetism in $BaCuSn_2$-$CeNi_{1-x}Si_2$-type YT_xGe_2 (T = Cr, Mn, Fe, Co, and Ni), J. Alloys Compd. **741**, 840 (2018).

[65] J. M. Lawrence, P. S. Riseborough, C. H. Booth, J. L. Sarrao, J. D. Thompson, and R. Osborn, Slow crossover in $YbXCu_4$ (X = Ag, Cd, In, Mg, Tl, Zn) intermediate-valence compounds, Phys. Rev. B **63**, 054427 (2001).

[66] A. N. Tahvildar-Zadeh, M. Jarrell, and J. K. Freericks, Protracted screening in the periodic Anderson model, Phys. Rev. B **55**, R3332(R) (1997).

[67] K. Ikeda and K. A. Gschneidner, Jr., Quenching of spin fluctuations by high magnetic fields in the heat capacity of $CeSn_3$, Phys. Rev. B **25**, 4623 (1982).

[68] K. Ikeda and K. A. Gschneidner Jr., Influence of high magnetic fields on the low temperature heat capacity of the itinerant electron ferromagnet Sc_3In, J. Magn. Magn. Mater. **30**, 273 (1983).

[69] T.-W. E. Tsang, K. A. Gschneidner, Jr., O. D. McMasters, R. J. Stierman, and S. K. Dhar, Anisotropic spin fluctuations in cubic $CeSn_3$, Phys. Rev. B **29**, 4185 (1984).